ACS Catalysis

Research Article

Cite This: ACS Catal. 2019, 9, 4958–4969

pubs.acs.org/acscatalysis

# Molecular Mechanisms of Oxygen Activation and Hydrogen Peroxide Formation in Lytic Polysaccharide Monooxygenases

Binju Wang,[†,▽] Paul H. Walton,*[,‡] and Carme Rovira*[,†,§]

[†]Departament de Química Inorgànica i Orgànica & IQTCUB, Universitat de Barcelona, Martí i Franquès 1, 08028 Barcelona, Spain

[‡]Department of Chemistry, University of York, Heslington, YO10 5DD, United Kingdom

[§]Institució Catalana de Recerca i Estudis Avançats (ICREA), Passeig Lluís Companys, 23, 08020 Barcelona, Spain

Supporting Information

**ABSTRACT:** Lytic polysaccharide monooxygenases (LPMOs) are copper-dependent enzymes for the degradation of recalcitrant polysaccharides such as chitin and cellulose. Unlike classical hydrolytic enzymes (cellulases), LPMOs catalyze the cleavage of the glycosidic bond via an oxidative mechanism using oxygen and a reductant. The full enzymatic molecular mechanisms, starting from the initial electron transfer from a reductant to oxygen activation and hydrogen peroxide formation, are not yet understood. Using quantum mechanics/molecular mechanics (QM/MM) metadynamics simulations, we have uncovered the oxygen activation mechanisms by LPMO in the presence of ascorbic acid, one of the most-used reductants in LPMOs assays. Our simulations capture the sequential formation of Cu(II)-$O_2^-$ and Cu(II)-$OOH^-$ intermediates via facile H atom abstraction from ascorbate. By investigating all the possible reaction pathways from the Cu(II)−$OOH^-$ intermediate, we ruled out Cu(II)-$O^{\bullet -}$ formation via direct O−O cleavage of Cu(II)-$OOH^-$. Meanwhile, we identified a possible pathway in which the proximal O atom of Cu(II)−$OOH^-$ abstracts a hydrogen atom from ascorbate, leading to Cu(I) and $H_2O_2$. The in-situ-generated $H_2O_2$ either converts to LPMO-Cu(II)-$O^{\bullet -}$ via a homolytic reaction, or diffuses into the bulk water in an uncoupled pathway. The competition of these two pathways is strongly dependent on the binding of the carbohydrate substrate, which plays a role in barricading the in-situ-generated $H_2O_2$ molecule, preventing its diffusion from the active site into the bulk water. Based on the present results, we propose a catalytic cycle of LPMOs that is consistent with the experimental information available. In particular, it explains the enigmatic substrate dependence of the reactivity of the LPMO with $H_2O_2$.

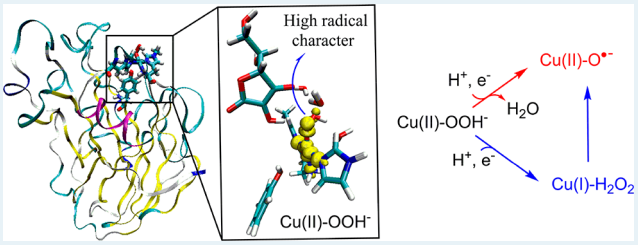


**KEYWORDS:** *Enzyme catalysis, lytic polysaccharide monooxygenases (LPMOs), $O_2$ activation, $H_2O_2$ formation, metadynamics*

## INTRODUCTION

Lytic polysaccharide monooxygenases (LPMOs) are regarded as the key enzymes for the degradation of polysaccharides such as chitin and cellulose,[1−16] being of high commercial interest in the production of biofuels. These enzymes activate glycosidic bonds through hydroxylation of the polysaccharide substrate at either the C1 or the C4 position, followed by the elimination of the scissile glycosidic bond and formation of the aldonic acids (Figure 1a) or 4-keto sugars at oxidized chain ends, respectively.[1−19]

As shown in Figure 1b, the LPMO active site contains a mononuclear copper center ligated by two histidine ligands (His1 and His78), an arrangement known as the histidine brace.[15] Figure 1a describes the general reaction catalyzed by LPMOs, in which two electrons are required to activate molecular oxygen toward the oxidative cleavage of polysaccharides. These two electrons are either externally supplied by small molecule reductants,[2−8,20] or enzymatic electron donors such as cellobiose dehydrogenase (CDH).[21] In most experiments, ascorbic acid has been used as an efficient electron donor for LPMOs.[2,4−8,20] Recent studies have shown that these enzymes may also use $H_2O_2$ as a co-substrate.[22−24] This finding is linked to the observation that LPMOs can generate $H_2O_2$ from uncoupled turnover when exposed to $O_2$ and a reducing agent in the absence of a substrate.[20,25,26]

Despite extensive experimental and computational studies, the molecular mechanism of LPMOs remains elusive, and sometimes even controversial.[16−19] Scheme 1 shows the putative catalytic pathways for the $O_2$-dependent activity of LPMOs that emerge from experimental and computational investigations. It is generally accepted that the catalytic cycle is entered via the one-electron reduction of the Cu(II) resting state to Cu(I), followed by $O_2$ binding to generate a Cu(II)-superoxo species, Cu(II)-$O_2^-$.[16−19,27] Early theoretical calculations[4] on small active site models suggested that $O_2$ binds in the axial coordination position, *trans* to the Tyr164 residue (see Figure 1b). However, a combined spectroscopic and computational study,[28] as well as QM/MM calculations[29] have

Received: February 21, 2019
Revised: April 17, 2019
Published: April 22, 2019




DOI: 10.1021/acscatal.9b00778
ACS Catal. 2019, 9, 4958−4969

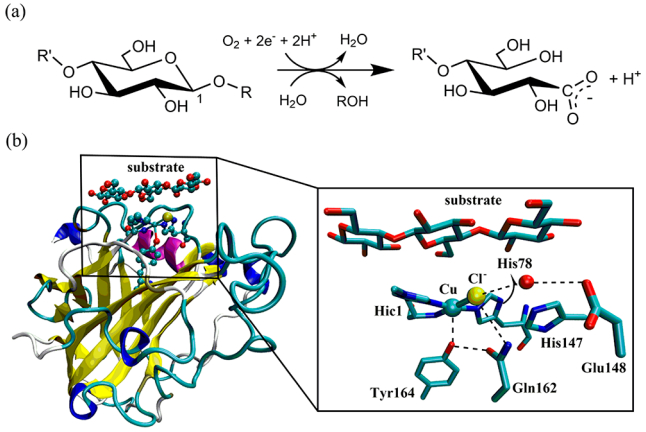


**Figure 1.** (a) General reaction for $O_2$-dependent activity of LPMOs toward oxidation at C1. (b) Crystal structure of LsAA9 LPMO with a polysaccharide substrate bound on the surface of the enzyme (PDB code: 5ACF). The right-side panel highlights the active site structure. Note that His1 is an $N_\delta$-methylated histidine (hereafter named Hic1) that is coordinated to the metal ion via both its imidazole $N_\varepsilon$ and its amino terminus NH2.

**Scheme 1. Possible Catalytic Pathways for the Polysaccharide Substrate Hydroxylation via the $O_2$-Dependent Activity of LPMOs**

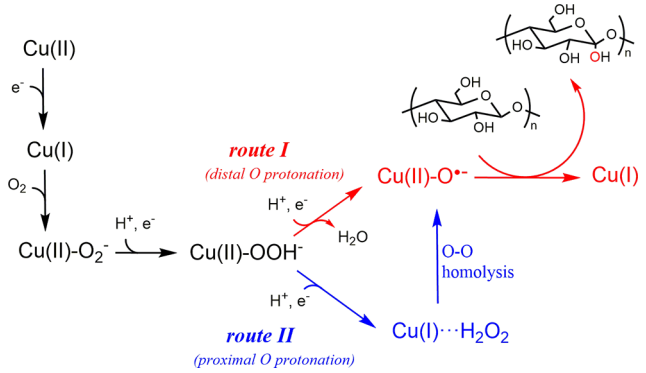


shown that the equatorial coordination is energetically more favorable. This is consistent with the recently determined crystal structure of a LPMO (CAZy classification AA9),[30] in which the polysaccharide substrate occupies the space around the axial position (Figure 1b), leaving only the equatorial site (occupied by a chloride exogenous ligand in the structure) for co-substrate binding.

The Cu(II)-$O_2^-$ species formed upon $O_2$ binding was initially proposed as the active one for the hydrogen atom abstraction (HAA) from the polysaccharide substrate,[4,31,32] but density functional theory (DFT) model calculations by Kim et al.[17] and, more recently, Bertini et al.[18] on the oxidation of "cellulosic" substrate by an AA9 LPMO have cast doubt on such a possibility. Since direct HAA from the substrate is unfavorable,[17,18] it is likely that the Cu(II)-$O_2^-$ species first converts to copper(II)-hydroperoxo [Cu(II)−$OOH^-$] (Scheme 1) by abstracting a H atom or via proton-coupled electron transfer (PCET) from a suitable co-substrate (e.g., ascorbate), depending on whether the electron and the proton are transferred simultaneously or separately, respectively.

Two distinct mechanistic routes can be envisaged for the reactivity of Cu(II)-$OOH^-$ in LPMO. Phillips et al.[4] proposed that a second electron transfer (coupled with distal O protonation) could facilitate the homolytic cleavage of the O−O bond, releasing a water molecule and forming a Cu−oxyl active species, Cu(II)-$O^{\bullet -}$ (route I in Scheme 1). Alternatively, Cu(II)-$OOH^-$ may react via its proximal O, leading to the formation of Cu(I) and $H_2O_2$ (route II in Scheme 1). In a recent work,[33] we demonstrated, in silico, that such Cu(I)-$H_2O_2$ species can evolve toward the reaction products. Specifically, $H_2O_2$ can be efficiently activated by LPMO-Cu(I) via a low-barrier homolysis mechanism, forming Cu(II)−OH and a caged hydroxyl radical intermediate (HO•) that evolves toward the highly reactive Cu(II)-$O^{\bullet -}$ species, which is the one oxidizing the polysaccharide substrate. However, it remains to be demonstrated whether Cu(I)···$H_2O_2$ is integral to the catalytic cycle (route II).

Although the reactivity of Cu(II)-$O^{\bullet -}$ is well-recognized, having been proposed as the active species of LPMO by computational studies,[17−19] the detailed molecular mechanism of $O_2$ activation and specifically the formation of this highly reactive species remains one of the most intriguing unanswered questions in LPMO catalysis. The full catalytic cycle (Scheme 1) involves several electron transfer steps that are mediated by a reductant. Therefore, the role of reductant is critical in the overall mechanism. From a computational perspective, however, reliable modeling of the reductant presents challenges, not least of which are those associated with accurate solvation energies of the reducing agent and the dynamic reorganization of the environment. Accordingly, electron-transfer related processes, such as electron transfer (ET), proton-coupled electron transfer (PCET), and hydrogen atom abstraction (HAA) involving the reductant have been somewhat neglected in previous mechanistic studies.[17−19] As a consequence, it is unknown whether any of the previously suggested mechanisms for $O_2$ activation is kinetically feasible.[17−19]

To address the above issues, we here employ a combination of molecular dynamics (MD) and QM/MM MD simulations to investigate the full $O_2$ activation mechanism of LPMOs in the presence of ascorbic acid, one of the most common reductants used in LPMO assays. Our results lead to the identification of a possible pathway in which Cu(I)···$H_2O_2$ forms during the catalytic cycle. Based on the present findings, a mechanism of LPMOs is proposed that explains the available experimental information and, in particular, the substrate dependence of the reactivity of the Cu(I)···$H_2O_2$ intermediate.

## METHODS

**System Setup.** The initial structure of LPMO was prepared on the basis of the recently determined crystal structure of the LPMO enzyme in complex with an oligosaccharide substrate (PDB code: 5ACF, with a resolution of 1.8 Å).[30] The substrate was removed from the structure and the equatorial $Cl^-$ ligand bound to Cu center was either replaced by $O_2$ (to model the Cu(II)-$O_2^-$ species) or by OOH (to model Cu(II)−$OOH^-$ species). We assigned the protonation states of titratable residues (His, Glu, Asp) on the basis of p$K_a$ values, using the PROPKA software[34] in combination with careful visual inspection of local hydrogen-bonded networks. Histidine residues His66, His78, His79, His125, and His131 were protonated at $N_\delta$, while His147 was protonated at $N_\delta$ and His122 was doubly protonated. All glutamic acid and aspartic acid residues were deprotonated. To investigate the possibility of His147 or Glu148 acting as proton donors during the reaction, these residues were selectively


DOI: 10.1021/acscatal.9b00778
ACS Catal. 2019, 9, 4958−4969

protonated. In these cases in which ascorbate was involved in the reaction, it was docked into the LPMO active site using the AutoDock Vina tool[35] in Chimera.[36] The general AMBER force field (GAFF)[37] was used for ascorbate, with the partial atomic charges obtained from the RESP model,[38] at the HF/6-31G* level of theory. The force field for the enzyme resting state, Cu(II)-$O_2^-$ and Cu(II)-$OOH^-$ states were parametrized using the "MCPB.py" modeling tool[39] of AmberTools16. The Amber ff14SB force field[40] was employed for the protein residues. Sodium ions were added to the protein surface to neutralize the total charge of the systems. Finally, the resulting system was solvated in a rectangular box of TIP3P waters extending up to a minimum distance of 18 Å from the protein surface.

**Classical MD Simulations.** After proper setup, the structures were fully minimized using a combination of steepest descent and conjugate gradients methods. The system was subsequently gently annealed from 10 K to 300 K in the canonical ensemble for 50 ps, using a weak restraint of 15 kcal/mol/Å on the protein backbone atoms. To achieve a uniform density after heating dynamics, 1 ns of density equilibration was performed under isothermal−isobaric ensemble at a target temperature and pressure of 300 K and 1.0 atm, respectively, using the Langevin thermostat[41] and the Berendsen barostats,[42] with collision frequency of 2 ps and pressure-relaxation time of 1 ps. Thereafter, all restraints were removed and the system was further equilibrated for 3 ns. Finally, a 50 ns production MD run was performed. In those cases in which either ascorbate or an $H_3O^+$ ion was involved in the reaction, their positions were restrained with a weak restraint of 5 kcal/mol/Å during equilibration and production MD simulations, avoiding that they diffuse into the bulk water. All MD simulations used the SHAKE algorithm, along with an integration step of 2 fs and they were performed with the GPU version of the Amber 16 package.[43]

**QM/MM MD and Metadynamics Simulations.** One representative snapshot extracted from each classical MD trajectory was used for the subsequent QM/MM MD simulation. All QM/MM MD simulations were performed with the CP2K 4.1 package,[44,45] combining the QM program QUICKSTEP[45] and the MM driver FIST. In this code, a real space multigrid technique is used to compute the electrostatic coupling between the QM and MM regions.[46,47] The QM region was treated at the DFT(B3LYP) level, employing a dual basis set of Gaussian and plane-waves (GPW) formalism,[45] whereas the MM region was modeled at the classical level using the same force-field as in the classical MD simulations. The QM region included at least the Cu cofactor, the Hic1 residue and the side chains of residues His78 and Tyr164. Gln162 was included in the QM region for those reactions in which this residue directly interacts either with $O_2$ or the OOH moiety. Other additional residues that were included for specific reactions are described in the manuscript. The wave function was expanded in a Gaussian double-$\zeta$ valence polarized (DZVP) basis set,[48] while an auxiliary plane-wave basis set with a cutoff of 360 Ry was used to converge the electron density, in conjunction with Goedecker−Teter−Hutter (GTH) pseudopotentials[49,50] for treating the core electrons. To accelerate the calculation of the Hartree−Fock exchange within B3LYP, the auxiliary density matrix method (ADMM) was used.[51] All QM/MM MD simulations were performed in the NVT ensemble using an integration time step of 0.5 fs. The systems were equilibrated without any constraint for 1.5 ps and the well-tempered metadynamics[52,53] method was used to explore the free-energy profile for each reaction step. Specific collective variables used for the different reaction steps are described in the manuscript. The width of the Gaussian-shaped potential hills was taken between 0.1 Å and 0.2 Å. The Gaussian height was set to 0.6 kcal/mol, while the time deposition interval between two consecutive Gaussians was set to 12.5 fs.

## RESULTS AND DISCUSSION

**Overview of the Redox Chemistry of Ascorbic Acid.** Ascorbic acid (Asc) or vitamin C is an important biological cofactor[54−57] and has been extensively used as an electron donor for the activity of LPMOs.[2,4−8,20] Its redox chemistry is summarized in Scheme 2. Ascorbic acid is a weak acid, with a

**Scheme 2. Summary of the Redox Chemistry of Ascorbic Acid, along with Computed Ionization Energy (IE, in kcal/mol) and Experimental p$K_a$ Values from ref 54**

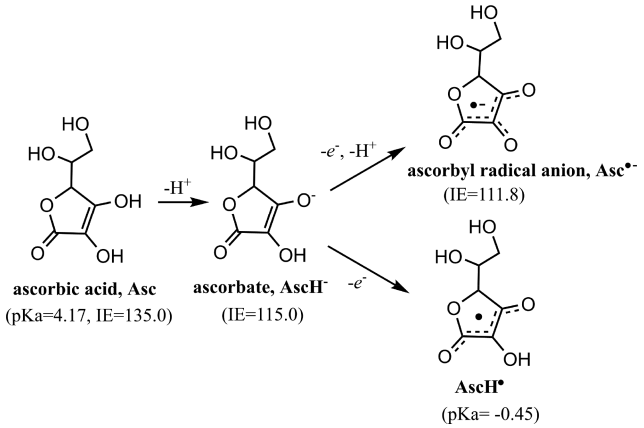


p$K_a$ of 4.17. Thus, it exists predominantly in the form of the ascorbate monoanion ($AscH^-$) at physiological pH and also at the pHs typically used in LPMO assays. The $AscH^-$ species is known to be a good electron donor, which either donates one electron to form the neutral ascorbyl radical (AscH•), or it simultaneously donates an electron and a proton to form the ascorbyl radical anion ($Asc^{\bullet -}$).[34] We computed the ionization energies (IEs) for the three possible electron donor species ($AscH^-$, AscH•, and, $Asc^{\bullet -}$, Scheme 2), and found that ascorbate ($AscH^-$) has the lowest ionization energy (see Table S1 in the Supporting Information), indicating that it is the most efficient one-electron donor, as suggested by experiments.

**Reduction of the Resting State LPMO-Cu(II) to Cu(I) by Ascorbate.** Since ascorbate is the predominant species and the most efficient one-electron donor, we first investigated the possible reduction of LPMO-Cu(II) by ascorbate (first step in Scheme 1). Calculation of the ionization energy of ascorbate ($AscH^-$) and the electron affinity of Cu(II) shows that removal of an electron from ascorbate requires an energy of 92.6 kcal/mol (see eq 1), while giving an electron to Cu(II) releases −114.5 kcal/mol (eq 2). Thus, the reduction of Cu(II) by ascorbate is expected to be thermodynamically quite favorable. This agrees with the experimental evidence that the LPMO-Cu (II) resting state can be reduced to Cu(I) in the presence of ascorbic acid.[27,58] Consistently, QM/MM MD simulations (see Figure S1 in the Supporting Information) of LPMO-Cu(II) in the presence of an ascorbate molecule show


DOI: 10.1021/acscatal.9b00778
ACS Catal. 2019, 9, 4958−4969

that there is a one-electron spin density located on the ascorbate molecule (Figure 2). This indicated that ascorbate

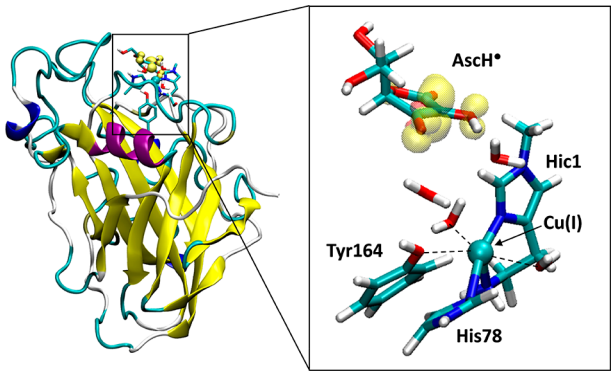


**Figure 2.** Structure of the QM region, along with the spin density distribution from QM/MM MD simulations starting from the resting state LPMO-Cu(II) in the presence of ascorbate.

has been oxidized to ascorbyl radical (AscH•), while Cu(II) has been reduced to Cu(I), as represented by eq 3. For comparison, we also investigated the alternative conformation, in which ascorbate is directly complexed with Cu(II). The resulting spin density (Figure S2 in the Supporting Information) shows that in this case $AscH^-$ is not able to transfer an electron to Cu(II). This suggests that water molecules play important roles in electron transfer, probably stabilizing the charge-separated product state.

$$AscH^- - e^- \rightarrow AscH\bullet \qquad \Delta E = 92.6\ \text{kcal/mol} \tag{1}$$

$$LPMO{-}Cu(II) + e^- \rightarrow LPMO{-}Cu(I) \qquad \Delta E = -114.5\ \text{kcal/mol} \tag{2}$$

$$LPMO{-}Cu(II) + AscH^- \rightarrow LPMO{-}Cu(I) + AscH\bullet \tag{3}$$

**Formation of Cu(II)-OOH$^-$.** Once Cu(II) has been reduced to Cu(I), molecular oxygen can bind to it in the equatorial position to form the Cu(II)-$O_2^-$ intermediate (the second step in Scheme 1), for which a triplet spin state has been determined.[17−19] As discussed above, ascorbate is a very good hydrogen donor,[54] so it is likely that Cu(II)-$O_2^-$ abstracts one H atom from an ascorbate molecule to generate Cu(II)-$OOH^-$. The O−H bond dissociation energy of ascorbate has been reported to be ∼73.6 kcal/mol,[54] while the computationally calculated C−H bond dissociation energy in a polysaccharide is >100 kcal/mol.[59] As such, abstracting a H atom from ascorbate is clearly much more favorable than from the polysaccharide substrate.

Figure 3a shows the QM/MM free-energy profile corresponding to the abstraction of one H atom from ascorbate by Cu(II)-$O_2^-$. The reaction is quite facile, with a free-energy barrier of 4.7 kcal/mol (Figure 3a). Analysis of the spin density population of the active site along the reaction (Figure 3b) reveals that two unpaired electrons are initially located on Cu(II) and $O_2^-$, respectively ($^3$**RC1**). Once ascorbate donates one H atom to Cu(II)-$O_2^-$, Cu(II)-$OOH^-$ and the anion ascorbyl radical ($Asc^{\bullet -}$) form ($^3$**IC1** in Figure 3a).

It could be argued that Cu(II)-$O_2^-$ abstracts an H atom from the neutral ascorbyl radical (AscH•) rather than ascorbate ($AscH^-$), leading to the same product Cu(II)-$OOH^-$ species. Our simulations predict this to be a facile process ($\Delta G^{\ddagger}$ = 1.8

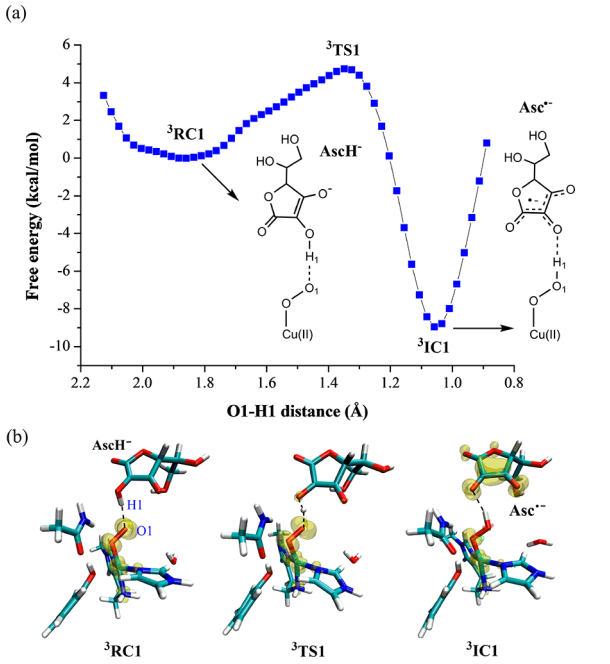


**Figure 3.** (a) Calculated free-energy profile for HAA from ascorbate by Cu(II)-$O_2^-$ species by QM/MM metadynamics. The reaction coordinate is defined as the distance between the O1 atom of Cu(II)-$O_2^-$ and the H1 atom of ascorbate. [Legend: RC = reactant complex, IC = intermediate complex, and TS = transition state.] (b) Representative structures of the QM region along the reaction pathway. Spin-up isodensity surfaces are plotted in yellow.

kcal/mol; see Figure S3 in the Supporting Information). However, $AscH^{\bullet}$ is a high-energy and highly acidic species ($pK_a$ = −0.45),[54] and it may rapidly dissociate in water before the HAA reaction. Thus, the most abundant and stable $AscH^-$ is more likely to be the predominant H atom donor for Cu(II)-$OOH^-$ generation, forming an ascorbyl radical anion ($Asc^{\bullet -}$). As the subsequent reaction step requires an additional H ($H^+$ + $e^-$), as indicated in Scheme 1, we can assume that the $Asc^{\bullet -}$ anion will exit the active site, being replaced by a fresh ascorbate molecule that can act as H atom donor, as required for the further reactivity of Cu(II)-$OOH^-$.

**Route I: Direct Formation of Cu(II)-O$^{\bullet -}$ from Cu(II)-OOH$^-$.** Starting from the LPMO-Cu(II)-$OOH^-$ + $AscH^-$ complex, we investigated the mechanism of Cu(II)-$O^{\bullet -}$ formation via direct O−O cleavage of Cu(II)-$OOH^-$ (route I in Scheme 1). Two possible pathways can be envisaged, depending whether the proton and electron required to cleave the O−O bond travel together (HAA) or separately (PCET). These two pathways are depicted in Scheme 3. All our attempts to abstract one hydrogen atom from ascorbate (Scheme 3a), coupled with O−O bond cleavage resulted in a free-energy barrier of at least 26 kcal/mol (Figure S4 in the Supporting Information), indicating that the HAA pathway is unfavorable.

Alternatively, protonation of the distal oxygen by an additional proton donor could be coupled with the transfer of one electron from ascorbate (Scheme 3b), triggering heterolytic O−O cleavage and formation of Cu(II)-$O^{\bullet -}$. This is a typical PCET process and requires an additional proton donor, in contrast to the HAA mechanism of Scheme 3a. The identity of the proton donor is elusive from all previous studies. Therefore, several species were tested as



DOI: 10.1021/acscatal.9b00778
ACS Catal. 2019, 9, 4958−4969

**Scheme 3. Two Possible Mechanisms for the Direct Formation of Cu(II)-O$^{\bullet -}$ from Cu(II)-OOH$^-$ (Pathway I in Scheme 1): (a) HAA-Mediated O−O Homolysis and (b) PCET-Mediated O−O Homolysis**

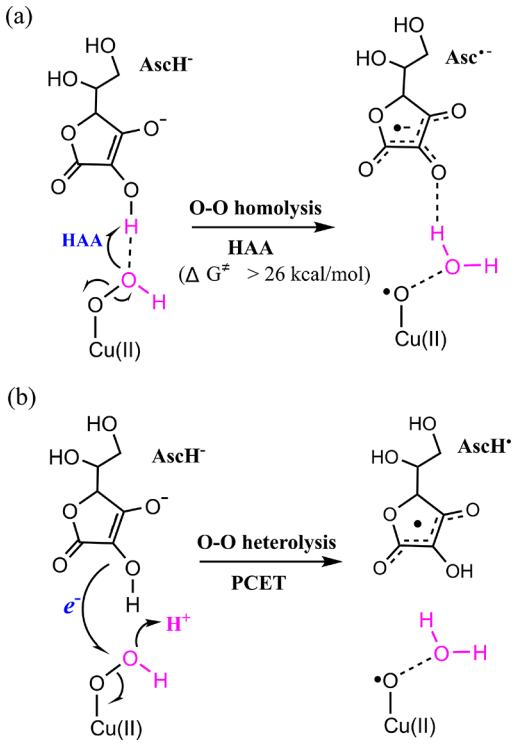


proton donor candidate (Scheme 4): protonated Glu148, a hydronium ion ($H_3O^+$) and ascorbic acid. His147 was not considered, in view of its low p$K_a$, as discussed later. None of these proton donors is likely to be stable or the dominating species at the optimal pH of LPMO[60] (see the discussion in the Supporting Information (section 2)). However, they may be present in small amounts, which may catalyze the PCET-mediated O−O heterolysis.

**Scheme 4. Three Possible Proton Donors That Could Be Involved in Cu(II)-O$^{\bullet -}$ Formation via the PCET-Mediated O−O Heterolysis of Cu(II)-OOH$^-$: (a) Protonated Glu148, (b) $H_3O^+$ Ion, and (c) Ascorbic Acid (Asc)**

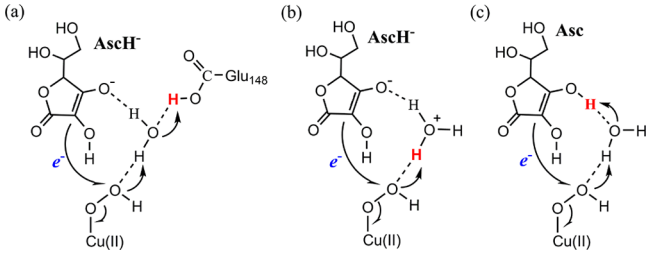


Glu148 is not in direct contact with the OOH moiety, thus proton transfer via its carboxylic acid side chain can only be mediated by a water molecule.[30] However, our simulations of LPMO-Cu(II)-OOH$^-$ with protonated Glu148 in the presence of ascorbate did not show any persistent water molecule between the distal oxygen of Cu(II)-OOH$^-$ and Glu148 that could play this role (Figure S5 in the Supporting Information). Thus, Glu148 can be excluded as a potential proton donor. Similarly, simulations considering $H_3O^+$ as a proton donor (Scheme 4b) showed that it rapidly donates one proton to ascorbate (within ∼100 fs; see Figures S6 and S7), leading to the more stable ascorbic acid species. Thus, the only possibility left is that PCET from ascorbic acid could catalyze the heterolytic cleavage of the O−O bond. QM/MM metadynamics simulations designed to drive the system from Cu(II)-OOH$^-$ to Cu(II)-O$^{\bullet -}$ (Figure 4) showed that, once the O−O bond breaks, not only the distal oxygen (O2) receives a proton from ascorbic acid (via the active site water molecule), but also the proximal oxygen spontaneously abstracts a hydrogen atom (HAA) from its closest ascorbic acid hydroxyl group, forming Cu(II)−OH$^-$ and dehydroascorbate (see Figure 4). In addition, the reaction requires a high free-energy barrier (29.6 kcal/mol), indicating that the ascorbic acid-mediated O−O cleavage of Cu(II)-OOH (route I in Scheme 1) is unfavorable.

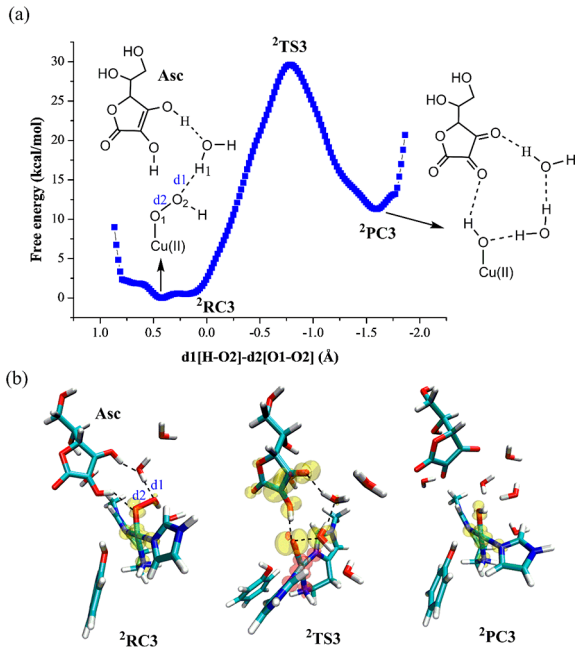


**Figure 4.** (a) Free-energy profile for PCET-mediated O−O heterolysis via ascorbic acid, obtained from QM/MM metadynamics. The reaction coordinate was defined as the distance difference between O2 and water H1 (d1) and that between O2 to O1 (d2). [Legend: RC = reactant complex, TS = transition state, and PC = product complex.] (b) Representative structures of the QM region along the reaction pathway. Spin-up and spin-down isodensity surfaces are plotted in yellow and red, respectively. At the transition state (**$^2$TS3**), a water molecule forms and one electron spin-density evolves on the ascorbic acid molecule. Nevertheless, the so-formed LPMO-Cu(II)-O$^{\bullet -}$/AscH• complex is quite unstable and Cu(II)-O$^{\bullet -}$ further abstracts a hydrogen atom from AscH•, leading to the more stable LPMO-Cu(II)−OH$^-$/dehydroascorbate product complex (**$^3$PC3**).

Note that the feasibility of Cu(II)-OOH$^-$ undergoing PCET is dependent on three main factors: cleavage of O−O bond, proton transfer to the distal O2, and electron transfer from ascorbate to Cu(II)-OOH$^-$. Among these factors, the first two are intrinsic to LPMO, while the third is dependent on the electron-donating efficiency of the reductant. Even though ascorbic acid is one of the most efficient small molecule electron donors, it is not able to trigger the PCET-mediated O−O heterolysis of Cu(II)-OOH$^-$, as demonstrated in this



DOI: 10.1021/acscatal.9b00778
ACS Catal. 2019, 9, 4958−4969

study. Thus, it is not expected that other small molecule reductants could be competent in LPMO catalysis. However, our work does not speak to how enzymatic electron donors like cellobiose dehydrogenase (CDH) work in LPMO.[4,10,21] If some "active" unpaired electrons can be generated or reserved for LPMOs during the action of CDH, the electron donor efficiency might be enhanced, which may reduce the energy barrier for PCET.

**Route II: Indirect Formation of Cu(II)-O$^{\bullet -}$ from Cu(II)-OOH$^-$ via the Cu(I)-$H_2O_2$ Intermediate.** In the above section, we ruled out all the possible pathways leading to Cu(II)-O$^{\bullet -}$ via the direct O−O cleavage of Cu(II)-OOH$^-$ (route I in Scheme 1). Here, we address the reactivity of Cu(II)-OOH$^-$ toward $H_2O_2$ formation (route II). For this to happen, it is necessary that the proximal O of Cu(II)-OOH$^-$ receives a proton (or a hydrogen atom). Two pathways can be envisaged, depending whether proton transfer (PT) or hydrogen atom abstraction (HAA) occurs (Scheme 5).

**Scheme 5. Three Possible Mechanistic Pathways for $H_2O_2$ Formation from Cu(II)-OOH$^-$ Species: (a) $H_2O_2$ Formation via the Proton Transfer to Proximal O of Cu(II)-OOH$^-$; (b) $H_2O_2$ Formation via HAA from Ascorbate by the Proximal O of Cu(II)-OOH$^-$; (c) $H_2O_2$ Formation via HAA from Tyr164 Residue by the Proximal O of Cu(II)-OOH$^-$**

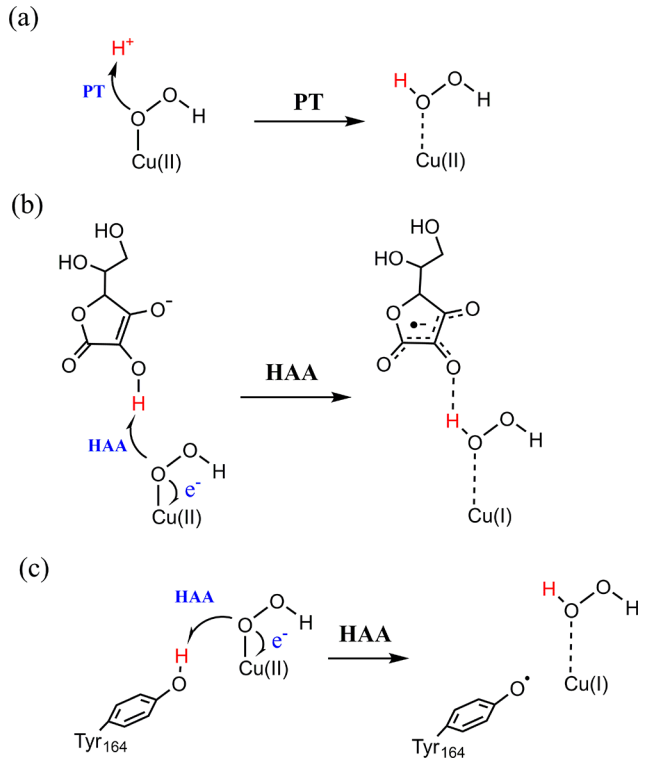


Protonation of the proximal O of Cu(II)-OOH$^-$ leads to the formation of $H_2O_2$ and Cu(II) (Scheme 5a). Alternatively, the proximal O of Cu(II)-OOH$^-$ may abstract a H atom from ascorbate or Tyr164, forming $H_2O_2$ and Cu(I) (see Schemes 5b and 5c).

Protonation of the proximal O of Cu(II)-OOH$^-$ (Scheme 5a) requires an appropriate proton donor in the active site, located near the proximal oxygen atom. The only residue that can play this role is His147, which is located ∼5 Å from Cu in the crystal structure.[30] This second-sphere residue has been suggested as a possible proton donor in a recent experimental study.[61] However, the calculated p$K_a$ of His147 is ∼3.5 (see the SI); therefore, it is expected to be in its neutral form at the optimal pH of 6.0−7.0 for LPMO, which is consistent with our previous study.[33] The local hydrogen-bond network of His147 is also consistent with it being singly protonated at $N_\varepsilon$. In fact, QM/MM metadynamics simulations starting with doubly protonated His147 show that such reaction does not lead to a stable product (Figure S8), ruling out $H_2O_2$ formation via the proton transfer pathway of Scheme 5a. Considering that the calculated p$K_a$ of His147 is very low (∼3.5), it is not expected that other residues would be able to mediate the $H_2O_2$ formation via the proton transfer of Scheme 5a.

The second mechanistic possibility is that Cu(II)-OOH$^-$ abstracts a H atom from ascorbate or Tyr164, forming $H_2O_2$ and Cu(I) (see Schemes 5b and 5c). Since ascorbate is both the dominant species and the efficient H atom donor, this reaction is expected to be feasible. Figure 5 shows the

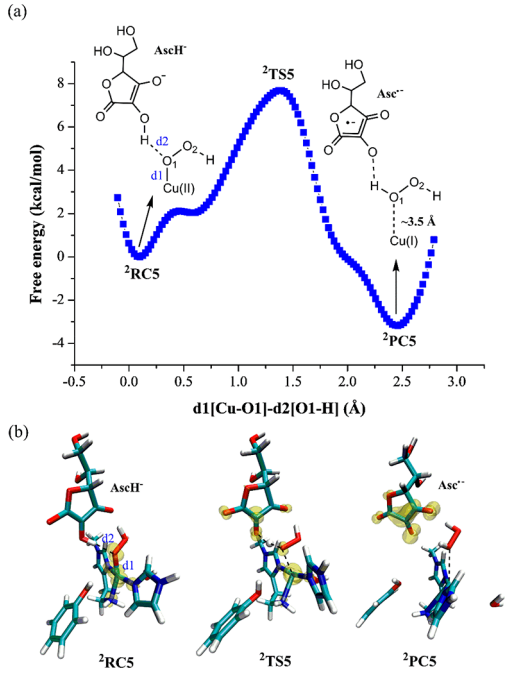


**Figure 5.** (a) Formation of $H_2O_2$ via HAA from ascorbate by the proximal O of Cu(II)-OOH$^-$, computed from QM/MM metadynamics. The reaction coordinate is defined as the distance difference between d1 (between Cu and O1 of water) and d2 (distance between O1 and H of ascorbate). **RC** = reactant complex, **TS** = transition state, **PC** = product complex. (b) Representative structures of the QM region along the reaction pathway. Spin-up isodensity surfaces are plotted in yellow.

computed free-energy profile, along with representative structures of the active site along the reaction pathway. There is a significant amount of spin density is located on the proximal O of Cu(II)-OOH$^-$ at the reactants state ($^2$**RC5**), suggesting this site may be efficient for the HAA reaction (Figure 5b). In fact, HAA from ascorbate by the proximal O of Cu(II)-OOH$^-$ involves a moderate barrier of ∼7.7 kcal/mol (Figure 5a), leading to the formation of $H_2O_2$ and an anion ascorbyl radical (Asc$^{\bullet -}$). The formation of Asc$^{\bullet -}$ is confirmed by analysis of the spin density ($^2$**PC5**). Very recently, QM/MM calculations[62] were performed to investigate the



DOI: 10.1021/acscatal.9b00778
ACS Catal. 2019, 9, 4958−4969

thermodynamics of $H_2O_2$ generation. In particular, it was found that $H_2O_2$ generation on LPMO-Cu(I), computed according to the reaction $O_2 + 2H^+ + 2e^- \rightarrow H_2O_2$, is thermodynamically favorable, which is consistent with our QM/MM MD-metadynamics results.

We also considered $H_2O_2$ formation via HAA from Tyr164 by the proximal O of Cu(II)-$OOH^-$(Scheme 5c). However, the calculated free-energy barrier turned out to be quite high (23.7 kcal/mol, see Figure S9 in the SI), the resulting $H_2O_2$ product complex is quite unstable (21.8 kcal/mol, relative to the initial reactant) and the reaction leads to a Tyr anion instead of the initially assumed Tyr radical. Clearly, Tyr164 is not efficient at mediating the $H_2O_2$ formation from Cu(II)-$OOH^-$ species.

Therefore, a thorough analysis of all possible reaction pathways leads to the conclusion that *the most likely reaction pathway from the Cu(II)-$OOH^-$intermediate is that in which its proximal oxygen atom abstracts a hydrogen atom from ascorbate, leading to $H_2O_2$ and Cu(I) (route II in Scheme 1)*. Afterwards, the Cu(I)-catalyzed O−O homolysis of $H_2O_2$ leads to the formation of Cu(II)-$O^{\bullet -}$, as demonstrated in our previous work.[33] In addition to ascorbate, we speculate that other reducing agents containing a redox-active hydroxyl group may activate the LPMO with similar mechanism to the one demonstrated herein. Thus, our findings may also explain the reactivity of other reducing co-substrates used in LPMO catalysis, such as gallate.[63,64]

**Is the Formation of Cu(II)-$O^{\bullet -}$ Catalyzed by His147?** During the writing of this manuscript, a QM/MM study in the absence of reductant appeared[19] in which the authors suggest that $O_2$ activation and Cu(II)-$O^{\bullet -}$ formation is catalyzed by the protonated His147 (as the proton donor), as shown in Scheme 6. In this mechanism, the protonation of Cu(II)-$O_2^-$

**Scheme 6. Proposed Mechanisms for $O_2$ Activation by LPMO from ref 6**

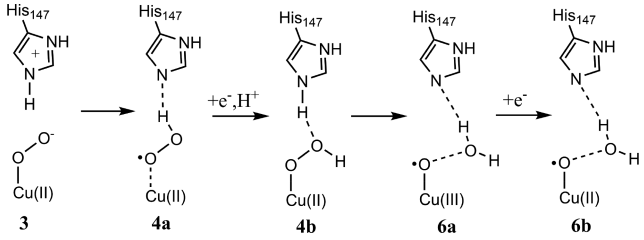


first leads to Cu(II) and a $HOO^{\bullet}$ radical (**4a**), followed by one-electron reduction to form Cu(II)-$OOH^-$ in a second protonation round from His147 (**4b**). Subsequently, proton transfer from His147 to the distal O of Cu(II)-$OOH^-$ triggers the heterolytic O−O cleavage of Cu(II)-$OOH^-$, leading to Cu(III)-$O^{\bullet -}$ (**6a**). A subsequent one-electron reduction generates the Cu(II)-$O^{\bullet -}$ reactive species (**6b**).

In principle, the generation of a high-energy Cu(III) product is expected to be an unfavorable process.[33] However, a low barrier of ∼10 kcal/mol was reported[19] for the proton-mediated O−O cleavage step (**4b** → **6a** in Scheme 6). Herein, we revisited this key step using the more advanced ab initio QM/MM MD simulations. Figure 6a shows the computed free-energy profile for the His147-catalyzed O−O heterolysis of Cu(II)-$OOH^-$, while Figure 6b shows the representative structures of the QM region along the reaction pathway. It can be seen that O1−O2 bond cleavage coupled with proton

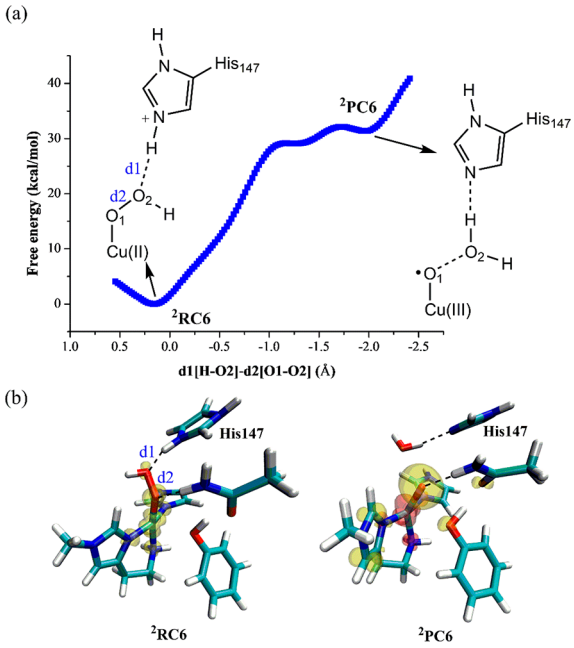


**Figure 6.** (a) Free-energy profile for His147-catalyzed O−O heterolysis of Cu(II)-$OOH^-$, obtained from QM/MM metadynamics. The reaction coordinate is defined as the distance difference between d1 (between O2 and H of His147) and d2 (between O2 to O1). [Legend: RC = reactant complex, PC = product complex.] (b) The representative structures of the QM region along the reaction pathway. Spin-up and spin-down isodensity surfaces are plotted in yellow and red, respectively.

transfer from His147 to O2 is highly unfavorable, involving an energy barrier >30 kcal/mol. Moreover, the so-formed "Cu(III)-$O^{\bullet -}$" product is a highly unstable species, corresponding to a very shallow minimum on the free-energy profile. Close inspection of the spin density population in $^2$PC6 reveals the precise electronic state of $^2$PC6. The spin-down unpaired electron (red isodensity) is located mostly on Cu (↓), arguing for a formal Cu(II) oxidation state. For the two spin-up unpaired electrons (yellow isodensity), one is located on O1 atom (↑), while the other is highly delocalized over Hic1, Tyr164 and Gln162 (↑). As such, the so-formed "Cu(III)-$O^{\bullet -}$" product is better described as [Hic + Tyr + Gln]$^{\bullet +}$—Cu(II)-$O^{\bullet -}$. Therefore, the Cu(III) product is quite unstable and abstracts an electron from the surrounding residues, oxidizing the enzyme. Overall, our calculations do not support the proton transfer-mediated heterolytic cleavage of Cu(II)-$OOH^-$ toward Cu(II)-$O^{\bullet -}$ formation, as it is kinetically highly unfavorable and would lead to the oxidation of the enzyme.

**Reactivity of LPMO−Cu(II)-$OOH^-$ vs Heme-Fe(III)-$OOH^-$.** It is interesting to compare the reactivity of the Cu(II)-$OOH^-$ intermediate in LPMO with that of heme enzymes. Heme enzymes, including P450[65,66] and heme peroxidases,[67,68] employ a well-established PCET mechanism to generate Fe(IV)−oxo porphyrin $\pi$-cation radical active species [Porph$^{\bullet +}$-Fe(IV)═O], denoted as compound I, from ferric hydroperoxide species [Porph-Fe(III)-$OOH^-$]. Why is the Cu(II)-$OOH^-$ species in LPMO not able to undergo a similar PCET-mediated O−O heterolysis?

As discussed above, the occurrence of the PCET mechanism is dependent on three factors: the O−O bond strength, the efficiency of proton transfer, and the efficiency of electron transfer. With respect to proton transfer, all these enzymes are



DOI: 10.1021/acscatal.9b00778
ACS Catal. 2019, 9, 4958−4969

similar, commonly using a protonated titratable residue (His, Glu, Asp) as proton donor. Concerning O−O bond strength, we predicted a O−O bond dissociation energy (BDE) of ∼40 kcal/mol for LPMO−Cu(II)-OOH$^-$, and ∼25 kcal/mol for P450−Fe(III)-OOH$^-$, respectively (see Figure S10 in the SI). Clearly, the O−O bond in LPMO−-Cu(II)-OOH$^-$ is much stronger than that in P450−Fe(III)-OOH$^-$. Considering electron transfer efficiency, it is known that heme P450 or peroxidases utilizes the porphyrin as the electron donor,[65−67,69,70] so the process is described as intramolecular electron transfer. By contrast, LPMO requires an external electron donor such as small molecule reductants or CDH,[16] which are featured as intermolecular electron transfer (Scheme 7). The kinetics of electron transfer are highly dependent on the coupling of the electron donor state and electron acceptor state[71] and it is expected that the electronic coupling is much stronger for intramolecular electron transfer than for intermolecular electron transfer. This explains why LPMO−Cu(II)-OOH$^-$ is less efficient for PCET-mediated O−O heterolysis than P450−Fe(III)-OOH$^-$.

**Scheme 7. Comparison between (a) the PCET-Mediated Cu(II)-O$^{\bullet -}$ Formation in LPMO and (b) the PCET-Mediated Cpd I Formation in P450**[a]

(a) **LPMO**

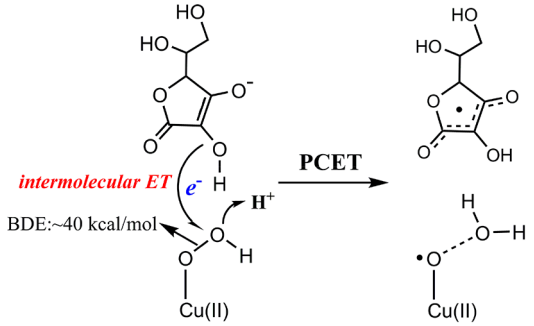


(b) **P450**

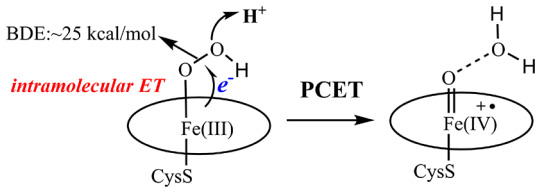


[a]Bond dissociation energies (BDEs) of O−O are given in units of kcal/mol. LPMO is featured as intermolecular electron transfer, while P450 is featured as intramolecular electron transfer.

Although the LPMO−Cu(II)-OOH$^-$ is too stable for O−O cleavage reactions (either homolysis or heterolysis), the unique radical character on its proximal O atom opens up reaction avenues toward HAA reactions. As demonstrated here, the proximal O of Cu(II)-OOH$^-$ can efficiently abstract a hydrogen atom from ascorbate, leading to the formation of $H_2O_2$ and Cu(I). Similarly, Cu(II)-OOH$^-$ could undergo HAA from active H atoms of biomass components, such as lignin, to activate LPMO. In fact, a boosting effect of lignin on the performance of LPMO has been observed by experiment.[72−75]

**Proposed Catalytic Cycle of LPMO.** Based on our present findings, we now propose a catalytic cycle of LPMO in the presence of ascorbate reductant (Scheme 8). This catalytic cycle is consistent with experimental data and furthermore

**Scheme 8. Full Catalytic Cycle of LPMO in the Presence of Ascorbic Acid Proposed in This Work**

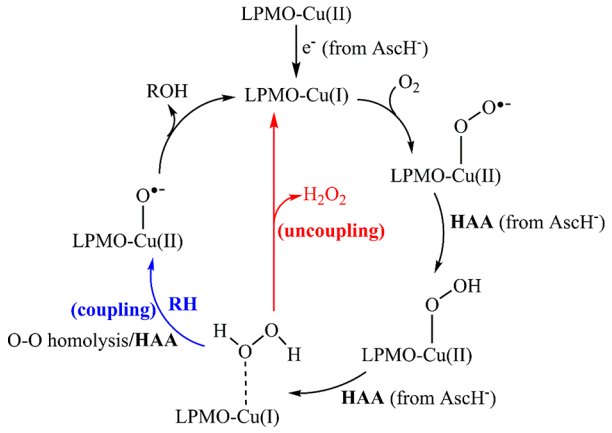


provides an explanation for the enigmatic substrate dependence of LPMO reactivity and hydrogen peroxide formation that is observed in the absence of substrate. Our proposal assumes that the association of LPMO with substrate during the reaction cycle is flexible at all stages of the reaction cycle, allowing access of both $O_2$ and reducing agent to the active site. Such dynamic processes have been experimentally demonstrated for LPMO-substrate-reducing agent interactions.[60]

Starting from the resting state of LPMO, Cu(II) undergoes the one-electron reduction to Cu(I) by ascorbate. This is followed by rapid $O_2$ binding to generate the LPMO−Cu(II)-$O_2^-$ species. Afterward, LPMO−Cu(II)-$O_2^-$ abstracts a hydrogen atom (HAA) from ascorbate to generate LPMO−Cu(II)-OOH$^-$. Starting from this species, our calculations uncovered an accessible pathway in which the proximal O of Cu(II)-OOH$^-$ abstracts a hydrogen atom from another ascorbate, leading to the formation of $H_2O_2$ and Cu(I). To check whether the bound substrate could interfere with $H_2O_2$ generation via HAA from ascorbate, QM/MM MD simulations were performed on the Cu(II)-OOH$^-$ species in the presence of both ascorbate and the polysaccharide substrate. The simulations indicate that ascorbate, via its redox-active hydroxyl group, has strong tendency to form a hydrogen bond with the proximal O of Cu-OOH. (See Figure 7, as well as Figure S11 in the SI.) This suggests that the binding of the polysaccharide substrate would have minor effects on $H_2O_2$ formation via HAA from ascorbate. The so-formed Cu(I)-$H_2O_2$ intermediate will either then convert to LPMO−Cu(II)-O$^{\bullet -}$ via the homolysis/HAA mechanism,[33] or lose $H_2O_2$ in the uncoupling pathway (see Scheme 8). The balance of these two pathways is critically dependent on the affinity of the LPMO for the substrate.

The competition of these two pathways (coupling versus uncoupling) is also dependent on the residence time of $H_2O_2$ in the active site of LPMO-Cu(I). According to our previous study,[33] the $H_2O_2$ co-substrate is bound to the active site of LPMO-Cu(I). Moreover, the active site of LPMO is exposed to bulk water. In such case, the binding of the substrate plays a key role in stabilizing $H_2O_2$ in the active site of LPMO−Cu(I). If a polysaccharide substrate is properly bound on the enzyme surface, $H_2O_2$ will be barricaded by the substrate and its



DOI: 10.1021/acscatal.9b00778
ACS Catal. 2019, 9, 4958−4969

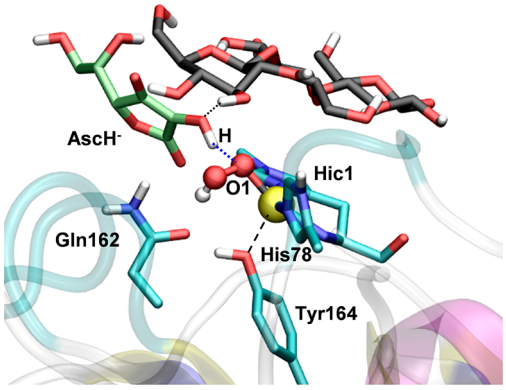


**Figure 7.** Structure of the LPMO−Cu(II)-$OOH^-$ intermediate in the presence of ascorbate and the polysaccharide substrate obtained from QM/MM MD simulations.

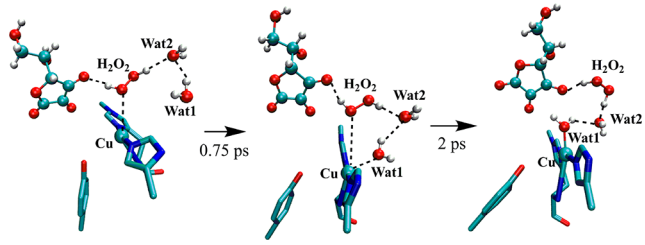


**Figure 8.** Movement of the $H_2O_2$ molecule in the LPMO active site in the absence of the polysaccharide substrate from QM/MM MD simulation. Representative structures extracted from the simulations ($^2$**PC5** state).

diffusion to the bulk water will be prevented. In such cases, the $H_2O_2$ molecule can be efficiently activated by LPMO-Cu(I) via a low-barrier homolysis/HAA mechanism, as previously demonstrated,[33] leading to the LPMO−Cu(II)-$O^{\bullet-}$ active species, which, in turn, oxidizes the substrate. This is the productive pathway, thus it can be called "coupling" pathway. However, in substrate-free LPMO, or when substrate binding is not effective enough, the hydrophilic $H_2O_2$ molecule may diffuse into the bulk water (uncoupling pathway in Scheme 8). This is in agreement with the experimental findings[20] that a "suitable" substrate could inhibit $H_2O_2$ generation and lead to a coupling reaction, while an "unsuitable" substrate, which is either too small or not fit for the active site of LPMO, may completely lead to an uncoupling reaction ($H_2O_2$ generation). Interestingly, such substrate-dependent reactivity of $H_2O_2$ in LPMO is quite similar to that of P450 heme enzymes, as previously demonstrated.[76]

The substrate-dependent reactivity of $H_2O_2$ described above is consistent with our present and past computational results. Our previous QM/MM optimized structure of LPMO−Cu(I)-$H_2O_2$ showed that $H_2O_2$ remains at a distance of 2.77 Å with Cu(I) in the presence of the polysaccharide substrate. We also found that the stabilization and reorientation of $H_2O_2$ in the active site is mainly controlled by second sphere residues such as His78, His147, Gln162, Glu148, and the substrate. In particular, the binding of the substrate has a tendency to block $H_2O_2$,[33] preventing its diffusion from the active site into the bulk water. In contrast, when the polysaccharide substrate is not present (Figure 5a) the so-generated $H_2O_2$ product ($^2$**PC5**) remains at a much longer distance (~3.5 Å) away from the Cu(I) center, suggesting that it could escape the active site.

To further reveal the dynamic movement of $H_2O_2$ in the absence of substrate, QM/MM MD simulations were performed on $^2$**PC5**. It was found that $H_2O_2$ moves away from Cu(I), while a nearby water (Wat1 in Figure 8) penetrates into the active site simutaneously. Finally, this water molecule binds weakly to Cu(I), while $H_2O_2$ remains separated from Cu(I) by two water molecules (Wat1 and Wat2). Thus, the in-situ-generated $H_2O_2$ molecule has a tendency to diffuse into the bulk water in the absence of substrate, which is quite facile, as predicted by our QM/MM MD simulations. In summary, the polysaccharide substrate not only barricades the $H_2O_2$ molecule, but also prevents the entry of bulk water molecules into the active site. As a consequence, the in-situ-generated $H_2O_2$ can further react with Cu(I) to form the Cu(II)-$O^{\bullet-}$ active species (via the "coupling" pathway in Scheme 8).

Our work and that of others[24,78] suggest that, in order to understand and then to develop $H_2O_2$-dependent LPMOs toward practical applications, one must consider both the substrate affinity to the active site and the possible hydrogen-bonding interactions between $H_2O_2$ and its surrounding residues. In particular, hydrophilic residues (e.g., Glu, Asp, His, Gln, or Asn) in the active site or located on the enzyme surface would favor both the $H_2O_2$ co-substrate and polysaccharide substrate binding, which, thus, may lead to efficient $H_2O_2$ activation. It is also conceivable that different LPMOs may exhibit different propensities in this regard.

## CONCLUSIONS

Using QM(B3LYP)/MM metadynamics simulations, we have uncovered the oxygen activation and $H_2O_2$ formation mechanisms in LPMOs in the presence of reductant ascorbic acid (Asc). Our simulations demonstrate that the resting state Cu(II) can be reduced to Cu(I) instantaneously in the presence of ascorbate. This is followed by $O_2$ binding to generate the LPMO−Cu(II)-$O_2^-$ species, which then perform a facile hydrogen atom abstraction (HAA) from ascorbate to generate LPMO−Cu(II)-$OOH^-$. As the O−H bond of ascorbate is much weaker than the C−H bond of polysaccharide, HAA from ascorbate is much more favorable than that from the polysaccharide substrate. Afterward, we investigated all possible reaction pathways starting from Cu(II)-$OOH^-$, and we were able to rule out any PCET- or proton transfer-mediated O−O cleavage mechanisms toward Cu(II)-$O^{\bullet-}$ formation. Meanwhile, we identified a possible pathway in which the proximal O of Cu(II)-$OOH^-$ abstracts a hydrogen atom from ascorbate, leading to the formation of $H_2O_2$ and Cu(I). The high radical character on the proximal O of Cu(II)-$OOH^-$ opens up reaction avenues toward HAA reactions, which may have implications in other copper-dependent enzymes.

Based on the present computational findings, a catalytic cycle of LPMOs is proposed in which $O_2$ is the oxidative co-substrate for LPMOs, from which an $H_2O_2$ intermediate is formed in situ via the activation of $O_2$ by reducing agents. Critically, the catalytic cycle explains the observed substrate dependence of the reactivity of the $H_2O_2$ intermediate, where the in-situ-generated $H_2O_2$ intermediate either converts to LPMO−Cu(II)-$O^{\bullet-}$ via the homolysis/HAA mechanism in a coupling pathway, or diffuses into the bulk water in an uncoupling pathway. The competition of these two pathways is dependent on the binding of substrate. A "suitable" substrate could barricade $H_2O_2$ and prevent $H_2O_2$ diffusion into the bulk


DOI: 10.1021/acscatal.9b00778
ACS Catal. 2019, 9, 4958−4969

water. Our results also speak to the ongoing debate about the activation of LPMOs by either $O_2$ or $H_2O_2$, showing that the two mechanistic pathways are connected. The present findings have far-reaching implications in $O_2$ activation and $H_2O_2$ formation mechanism by other copper enzymes.[77]

## ■ ASSOCIATED CONTENT

### Supporting Information

The Supporting Information is available free of charge on the ACS Publications website at DOI: 10.1021/acscatal.9b00778.

Additional QM(B3LYP)/MM metadynamics simulations and QM(B3LYP)/MM MD simulations results (PDF)

## ■ AUTHOR INFORMATION


### Corresponding Authors

*E-mail: paul.walton@york.ac.uk (P. H. Walton).
*E-mail: c.rovira@ub.edu (C. Rovira).

### ORCID

Paul H. Walton: 0000-0002-1152-1480
Carme Rovira: 0000-0003-1477-5010

### Present Address

[∇]State Key Laboratory of Physical Chemistry of Solid Surfaces and Fujian Provincial Key Laboratory of Theoretical and Computational Chemistry, College of Chemistry and Chemical Engineering, Xiamen University, Xiamen 360015, PRC.


### Notes

The authors declare no competing financial interest.

## ■ ACKNOWLEDGMENTS

This work was supported by grants from MINECO (No. CTQ2017-85496-P, to C.R.), AGAUR (No. 2017SGR-1189, to C.R.), the Spanish Structures of Excellence María de Maeztu (No. MDM-2017-0767, to C.R.), and Biotechnology and Biological Sciences Research Council (BBSRC) (No. BB/R007705/1 to P. H. W.). The authors gratefully acknowledge the computer resources at MareNostrum and Minotauro, as well as the technical support provided by BSC−CNS (No. RES-QCM-2019-1-0020). B.W. thanks AGAUR for a Beatriu de Pinós postdoctoral fellowship (No. 2016BP-00206). Dr. Marcella Iannuzzi and Pablo Campomanes are acknowledged for technical suggestions. We also thank Prof. Gideon J. Davies for insightful discussions.

## ■ DEDICATION

This manuscript is dedicated to Prof. Sason Shaik, on the occasion of his 70th Birthday.

## ■ REFERENCES


(1) Harris, P. V.; Welner, D.; McFarland, K. C.; Re, E.; Navarro Poulsen, J. C.; Brown, K.; Salbo, R.; Ding, H.; Vlasenko, E.; Merino, S.; Xu, F.; Cherry, J.; Larsen, S.; Lo Leggio, L. Stimulation of lignocellulosic biomass hydrolysis by proteins of glycoside hydrolase family 61: structure and function of a large, enigmatic family. *Biochemistry* **2010**, *49*, 3305−3316.

(2) Vaaje-Kolstad, G.; Westereng, B.; Horn, S. J.; Liu, Z.; Zhai, H.; Sorlie, M.; Eijsink, V. G. An oxidative enzyme boosting the enzymatic conversion of recalcitrant polysaccharides. *Science* **2010**, *330*, 219−222.

(3) Quinlan, R. J.; Sweeney, M. D.; Lo Leggio, L.; Otten, H.; Poulsen, J. C.; Johansen, K. S.; Krogh, K. B.; Jorgensen, C. I.; Tovborg, M.; Anthonsen, A.; Tryfona, T.; Walter, C. P.; Dupree, P.; Xu, F.; Davies, G. J.; Walton, P. H. Insights into the oxidative degradation of cellulose by a copper metalloenzyme that exploits biomass components. *Proc. Natl. Acad. Sci. U. S. A.* **2011**, *108*, 15079−15084.

(4) Phillips, C. M.; Beeson, W. T.; Cate, J. H.; Marletta, M. A. Cellobiose dehydrogenase and a copper-dependent polysaccharide monooxygenase potentiate cellulose degradation by Neurospora crassa. *ACS Chem. Biol.* **2011**, *6*, 1399−1406.

(5) Beeson, W. T.; Phillips, C. M.; Cate, J. H.; Marletta, M. A. Oxidative cleavage of cellulose by fungal copper-dependent polysaccharide monooxygenases. *J. Am. Chem. Soc.* **2012**, *134*, 890−892.

(6) Hemsworth, G. R.; Henrissat, B.; Davies, G. J.; Walton, P. H. Discovery and characterization of a new family of lytic polysaccharide monooxygenases. *Nat. Chem. Biol.* **2014**, *10*, 122−126.

(7) Lo Leggio, L.; Simmons, T. J.; Poulsen, J. C.; Frandsen, K. E.; Hemsworth, G. R.; Stringer, M. A.; von Freiesleben, P.; Tovborg, M.; Johansen, K. S.; De Maria, L.; Harris, P. V.; Soong, C. L.; Dupree, P.; Tryfona, T.; Lenfant, N.; Henrissat, B.; Davies, G. J.; Walton, P. H. Structure and boosting activity of a starch-degrading lytic polysaccharide monooxygenase. *Nat. Commun.* **2015**, *6*, 5961.

(8) Vu, V. V.; Beeson, W. T.; Phillips, C. M.; Cate, J. H.; Marletta, M. A. Determinants of regioselective hydroxylation in the fungal polysaccharide monooxygenases. *J. Am. Chem. Soc.* **2014**, *136*, 562−565.

(9) Tan, T. C.; Kracher, D.; Gandini, R.; Sygmund, C.; Kittl, R.; Haltrich, D.; Hallberg, B. M.; Ludwig, R.; Divne, C. Structural basis for cellobiose dehydrogenase action during oxidative cellulose degradation. *Nat. Commun.* **2015**, *6*, 7542.

(10) Cannella, D.; Mollers, K. B.; Frigaard, N. U.; Jensen, P. E.; Bjerrum, M. J.; Johansen, K. S.; Felby, C. Light-driven oxidation of polysaccharides by photosynthetic pigments and a metalloenzyme. *Nat. Commun.* **2016**, *7*, 11134.

(11) Horn, S. J.; Vaaje-Kolstad, G.; Westereng, B.; Eijsink, V. G. Novel enzymes for the degradation of cellulose. *Biotechnol. Biofuels* **2012**, *5*, 45.

(12) Hemsworth, G. R.; Davies, G. J.; Walton, P. H. Recent insights into copper-containing lytic polysaccharide mono-oxygenases. *Curr. Opin. Struct. Biol.* **2013**, *23*, 660−668.

(13) Walton, P. H.; Davies, G. J. On the catalytic mechanisms of lytic polysaccharide monooxygenases. *Curr. Opin. Chem. Biol.* **2016**, *31*, 195−207.

(14) Vaaje-Kolstad, G.; Forsberg, Z.; Loose, J. S.; Bissaro, B.; Eijsink, V. G. Structural diversity of lytic polysaccharide monooxygenases. *Curr. Opin. Struct. Biol.* **2017**, *44*, 67−76.

(15) Ciano, L.; Davies, G. J.; Tolman, W. B.; Walton, P. H. Bracing copper for the catalytic oxidation of C−H bonds. *Nat. Catal.* **2018**, *1*, 571−577.

(16) Meier, K. K.; Jones, S. M.; Kaper, T.; Hansson, H.; Koetsier, M. J.; Karkehabadi, S.; Solomon, E. I.; Sandgren, M.; Kelemen, B. Oxygen Activation by Cu LPMOs in Recalcitrant Carbohydrate Polysaccharide Conversion to Monomer Sugars. *Chem. Rev.* **2018**, *118*, 2593−2635.

(17) Kim, S.; Stahlberg, J.; Sandgren, M.; Paton, R. S.; Beckham, G. T. Quantum mechanical calculations suggest that lytic polysaccharide monooxygenases use a copper-oxyl, oxygen-rebound mechanism. *Proc. Natl. Acad. Sci. U. S. A.* **2014**, *111*, 149−154.

(18) Bertini, L.; Breglia, R.; Lambrughi, M.; Fantucci, P.; De Gioia, L.; Borsari, M.; Sola, M.; Bortolotti, C. A.; Bruschi, M. Catalytic Mechanism of Fungal Lytic Polysaccharide Monooxygenases Investigated by First-Principles Calculations. *Inorg. Chem.* **2018**, *57*, 86−97.

(19) Hedegard, E. D.; Ryde, U. Molecular mechanism of lytic polysaccharide monooxygenases. *Chem. Sci.* **2018**, *9*, 3866−3880.

(20) Isaksen, T.; Westereng, B.; Aachmann, F. L.; Agger, J. W.; Kracher, D.; Kittl, R.; Ludwig, R.; Haltrich, D.; Eijsink, V. G.; Horn, S. J. A C4-oxidizing lytic polysaccharide monooxygenase cleaving both cellulose and cello-oligosaccharides. *J. Biol. Chem.* **2014**, *289*, 2632−2642.




DOI: 10.1021/acscatal.9b00778
*ACS Catal.* 2019, 9, 4958−4969

(21) Kracher, D.; Scheiblbrandner, S.; Felice, A. K.; Breslmayr, E.; Preims, M.; Ludwicka, K.; Haltrich, D.; Eijsink, V. G.; Ludwig, R. Extracellular electron transfer systems fuel cellulose oxidative degradation. *Science* **2016**, *352*, 1098−1101.
(22) Bissaro, B.; Rohr, A. K.; Muller, G.; Chylenski, P.; Skaugen, M.; Forsberg, Z.; Horn, S. J.; Vaaje-Kolstad, G.; Eijsink, V. G. H. Oxidative cleavage of polysaccharides by monocopper enzymes depends on $H_2O_2$. *Nat. Chem. Biol.* **2017**, *13*, 1123−1128.
(23) Kuusk, S.; Bissaro, B.; Kuusk, P.; Forsberg, Z.; Eijsink, V. G. H.; Sorlie, M.; Valjamae, P. Kinetics of $H_2O_2$-driven degradation of chitin by a bacterial lytic polysaccharide monooxygenase. *J. Biol. Chem.* **2018**, *293*, 523−531.
(24) Hangasky, J. A.; Iavarone, A. T.; Marletta, M. A. Reactivity of O2 versus $H_2O_2$ with polysaccharide monooxygenases. *Proc. Natl. Acad. Sci. U. S. A.* **2018**, *115*, 4915−4920.
(25) Kittl, R.; Kracher, D.; Burgstaller, D.; Haltrich, D.; Ludwig, R. Production of four Neurospora crassa lytic polysaccharide monooxygenases in Pichia pastoris monitored by a fluorimetric assay. *Biotechnol. Biofuels* **2012**, *5*, 79.
(26) Scott, B. R.; Huang, H. Z.; Frickman, J.; Halvorsen, R.; Johansen, K. S. Catalase improves saccharification of lignocellulose by reducing lytic polysaccharide monooxygenase-associated enzyme inactivation. *Biotechnol. Lett.* **2016**, *38*, 425−434.
(27) O'Dell, W. B.; Agarwal, P. K.; Meilleur, F. Oxygen Activation at the Active Site of a Fungal Lytic Polysaccharide Monooxygenase. *Angew. Chem., Int. Ed.* **2017**, *56*, 767−770.
(28) Kjaergaard, C. H.; Qayyum, M. F.; Wong, S. D.; Xu, F.; Hemsworth, G. R.; Walton, D. J.; Young, N. A.; Davies, G. J.; Walton, P. H.; Johansen, K. S.; Hodgson, K. O.; Hedman, B.; Solomon, E. I. Spectroscopic and computational insight into the activation of O2 by the mononuclear Cu center in polysaccharide monooxygenases. *Proc. Natl. Acad. Sci. U. S. A.* **2014**, *111*, 8797−8802.
(29) Hedegård, E. D.; Ryde, U. Multiscale Modelling of Lytic Polysaccharide Monooxygenases. *ACS Omega.* **2017**, *2*, 536−545.
(30) Frandsen, K. E.; Simmons, T. J.; Dupree, P.; Poulsen, J. C.; Hemsworth, G. R.; Ciano, L.; Johnston, E. M.; Tovborg, M.; Johansen, K. S.; von Freiesleben, P.; Marmuse, L.; Fort, S.; Cottaz, S.; Driguez, H.; Henrissat, B.; Lenfant, N.; Tuna, F.; Baldansuren, A.; Davies, G. J.; Lo Leggio, L.; Walton, P. H. The molecular basis of polysaccharide cleavage by lytic polysaccharide monooxygenases. *Nat. Chem. Biol.* **2016**, *12*, 298−303.
(31) Li, X.; Beeson, W. T. T.; Phillips, C. M.; Marletta, M. A.; Cate, J. H. Structural basis for substrate targeting and catalysis by fungal polysaccharide monooxygenases. *Structure* **2012**, *20*, 1051−1061.
(32) Beeson, W. T.; Vu, V. V.; Span, E. A.; Phillips, C. M.; Marletta, M. A. Cellulose degradation by polysaccharide monooxygenases. *Annu. Rev. Biochem.* **2015**, *84*, 923−946.
(33) Wang, B.; Johnston, E. M.; Li, P.; Shaik, S.; Davies, G. J.; Walton, P. H.; Rovira, C. QM/MM Studies into the $H_2O_2$-Dependent Activity of Lytic Polysaccharide Monooxygenases: Evidence for the Formation of a Caged Hydroxyl Radical Intermediate. *ACS Catal.* **2018**, *8*, 1346−1351.
(34) Olsson, M. H. M.; Søndergaard, C. R.; Rostkowski, M.; Jensen, J. H. PROPKA3: Consistent Treatment of Internal and Surface Residues in Empirical pKa Predictions. *J. Chem. Theory Comput.* **2011**, *7*, 525−537.
(35) Trott, O.; Olson, A. J. AutoDock Vina: improving the speed and accuracy of docking with a new scoring function, efficient optimization, and multithreading. *J. Comput. Chem.* **2010**, *31*, 455−461.
(36) Pettersen, E. F.; Goddard, T. D.; Huang, C. C.; Couch, G. S.; Greenblatt, D. M.; Meng, E. C.; Ferrin, T. E. UCSF Chimera–a visualization system for exploratory research and analysis. *J. Comput. Chem.* **2004**, *25*, 1605−1612.
(37) Wang, J. M.; Wolf, R. M.; Caldwell, J. W.; Kollman, P. A.; Case, D. A. Development and testing of a general amber force field. *J. Comput. Chem.* **2004**, *25*, 1157−1174.
(38) Bayly, C. I.; Cieplak, P.; Cornell, W. D.; Kollman, P. A. A well-behaved electrostatic potential based method using charge restraints for deriving atomic charges. The RESP model. *J. Phys. Chem.* **1993**, *97*, 10269−10280.
(39) Li, P.; Merz, K. M., Jr. MCPB.py: A Python Based Metal Center Parameter Builder. *J. Chem. Inf. Model.* **2016**, *56*, 599−604.
(40) Maier, J. A.; Martinez, C.; Kasavajhala, K.; Wickstrom, L.; Hauser, K. E.; Simmerling, C. ff14SB: Improving the Accuracy of Protein Side Chain and Backbone Parameters from ff99SB. *J. Chem. Theory Comput.* **2015**, *11*, 3696−3713.
(41) Izaguirre, J. A.; Catarello, D. P.; Wozniak, J. M.; Skeel, R. D. Langevin stabilization of molecular dynamics. *J. Chem. Phys.* **2001**, *114*, 2090−2098.
(42) Berendsen, H. J. C.; Postma, J. P. M.; van Gunsteren, W. F.; DiNola, A.; Haak, J. R. Molecular dynamics with coupling to an external bath. *J. Chem. Phys.* **1984**, *81*, 3684−3690.
(43) Case, D. A.; Cerutti, D. S.; Cheatham, T. E., III; Darden, T. A.; Duke, R. E.; Giese, T. J.; Gohlke, H.; Goetz, A. W.; Greene, D.; Homeyer, N.; Izadi, S.; Kovalenko, A.; Lee, T. S.; LeGrand, S.; Li, P.; Lin, C.; Liu, J.; Luchko, T.; Luo; Mermelstein, D.; Merz, K. M.; Monard, G.; Nguyen, H.; Omelyan, I.; Onufriev, A.; Pan, F.; Qi, R.; Roe, D. R.; Roitberg, A.; Sagui, C.; Simmerling, C. L.; Botello-Smith, W. M.; Swails, J.; Walker, R. C.; Wang, J.; Wolf, R. M.; Wu, X.; Xiao, L.; York, D. M.; Kollman, P. A. *AMBER 2017.*; University of California, San Francisco, CA, 2017.
(44) CP2K version 4.1, the CP2K developers group, 2016 CP2K is freely available from https://www.cp2k.org.
(45) VandeVondele, J.; Krack, M.; Mohamed, F.; Parrinello, M.; Chassaing, T.; Hutter, J. Quickstep: Fast and accurate density functional calculations using a mixed Gaussian and plane waves approach. *Comput. Phys. Commun.* **2005**, *167*, 103−128.
(46) Laino, T.; Mohamed, F.; Laio, A.; Parrinello, M. An Efficient Real Space Multigrid QM/MM Electrostatic Coupling. *J. Chem. Theory Comput.* **2005**, *1*, 1176−1184.
(47) Laio, A.; VandeVondele, J.; Rothlisberger, U. A Hamiltonian electrostatic coupling scheme for hybrid Car-Parrinello molecular dynamics simulations. *J. Chem. Phys.* **2002**, *116*, 6941−6947.
(48) VandeVondele, J.; Hutter, J. Gaussian basis sets for accurate calculations on molecular systems in gas and condensed phases. *J. Chem. Phys.* **2007**, *127*, 114105.
(49) Goedecker, S.; Teter, M.; Hutter, J. Separable dual-space Gaussian pseudopotentials. *Phys. Rev. B: Condens. Matter Mater. Phys.* **1996**, *54*, 1703−1710.
(50) Hartwigsen, C.; Goedecker, S.; Hutter, J. Relativistic separable dual-space Gaussian pseudopotentials from H to Rn. *Phys. Rev. B: Condens. Matter Mater. Phys.* **1998**, *58*, 3641−3662.
(51) Guidon, M.; Hutter, J.; VandeVondele, J. Auxiliary Density Matrix Methods for Hartree-Fock Exchange Calculations. *J. Chem. Theory Comput.* **2010**, *6*, 2348−2364.
(52) Laio, A.; Parrinello, M. Escaping free-energy minima. *Proc. Natl. Acad. Sci. U. S. A.* **2002**, *99*, 12562−12566.
(53) Barducci, A.; Bussi, G.; Parrinello, M. Well-tempered metadynamics: a smoothly converging and tunable free-energy method. *Phys. Rev. Lett.* **2008**, *100*, 020603.
(54) Warren, J. J.; Mayer, J. M. Tuning of the thermochemical and kinetic properties of ascorbate by its local environment: solution chemistry and biochemical implications. *J. Am. Chem. Soc.* **2010**, *132*, 7784−7793.
(55) *Vitamin C in Health and Disease*; Packer, L., Fuchs, J., Eds.; Marcel Dekker: New York, 1997; Vol. *5*.
(56) Njus, D.; Wigle, M.; Kelley, P. M.; Kipp, B. H.; Schlegel, H. B. Mechanism of ascorbic acid oxidation by cytochrome $b_{561}$. *Biochemistry* **2001**, *40*, 11905−11911.
(57) Agathocleous, M.; Meacham, C. E.; Burgess, R. J.; Piskounova, E.; Zhao, Z.; Crane, G. M.; Cowin, B. L.; Bruner, E.; Murphy, M. M.; Chen, W.; Spangrude, G. J.; Hu, Z.; DeBerardinis, R. J.; Morrison, S. J. Ascorbate regulates haematopoietic stem cell function and leukaemogenesis. *Nature* **2017**, *549*, 476−481.
(58) Hemsworth, G. R.; Taylor, E. J.; Kim, R. Q.; Gregory, R. C.; Lewis, S. J.; Turkenburg, J. P.; Parkin, A.; Davies, G. J.; Walton, P. H.


DOI: 10.1021/acscatal.9b00778
*ACS Catal.* 2019, 9, 4958−4969

The copper active site of CBM33 polysaccharide oxygenases. *J. Am. Chem. Soc.* **2013**, *135*, 6069−6077.
(59) Hedegard, E. D.; Ryde, U. Targeting the reactive intermediate in polysaccharide monooxygenases. *JBIC, J. Biol. Inorg. Chem.* **2017**, *22*, 1029−1037.
(60) Hangasky, J. A.; Marletta, M. A. A Random-Sequential Kinetic Mechanism for Polysaccharide Monooxygenases. *Biochemistry* **2018**, *57*, 3191−3199.
(61) Span, E. A.; Suess, D. L. M.; Deller, M. C.; Britt, R. D.; Marletta, M. A. The Role of the Secondary Coordination Sphere in a Fungal Polysaccharide Monooxygenase. *ACS Chem. Biol.* **2017**, *12*, 1095−1103.
(62) Caldararu, O.; Oksanen, E.; Ryde, U.; Hedegård, E. D. Mechanism of hydrogen peroxide formation by lytic polysaccharide monooxygenase. *Chem. Sci.* **2019**, *10*, 576−686.
(63) Hu, J.; Arantes, V.; Pribowo, A.; Gourlay, K.; Saddler, J. N. Substrate factors that influence the synergistic interaction of AA9 and cellulases during the enzymatic hydrolysis of biomass. *Energy Environ. Sci.* **2014**, *7*, 2308−2315.
(64) Hu, J.; Tian, D.; Renneckar, S.; Saddler, J. N. Enzyme mediated nanofibrillation of cellulose by the synergistic actions of an endoglucanase, lytic polysaccharide monooxygenase (LPMO) and xylanase. *Sci. Rep.* **2018**, *8*, 3195.
(65) Zheng, J.; Wang, D.; Thiel, W.; Shaik, S. QM/MM study of mechanisms for compound I formation in the catalytic cycle of cytochrome P450cam. *J. Am. Chem. Soc.* **2006**, *128*, 13204−13215.
(66) Shaik, S.; Cohen, S.; Wang, Y.; Chen, H.; Kumar, D.; Thiel, W. P450 enzymes: their structure, reactivity, and selectivity-modeled by QM/MM calculations. *Chem. Rev.* **2010**, *110*, 949−1017.
(67) Derat, E.; Shaik, S.; Rovira, C.; Vidossich, P.; Alfonso-Prieto, M. The effect of a water molecule on the mechanism of formation of compound 0 in horseradish peroxidase. *J. Am. Chem. Soc.* **2007**, *129*, 6346−6347.
(68) Vidossich, P.; Fiorin, G.; Alfonso-Prieto, M.; Derat, E.; Shaik, S.; Rovira, C. On the role of water in peroxidase catalysis: a theoretical investigation of HRP compound I formation. *J. Phys. Chem. B* **2010**, *114*, 5161−5169.
(69) Vidossich, P.; Alfonso-Prieto, M.; Carpena, X.; Loewen, P. C.; Fita, I.; Rovira, C. Versatility of the electronic structure of compound I in catalase-peroxidases. *J. Am. Chem. Soc.* **2007**, *129*, 13436−13446.
(70) Poulos, T. L. Heme enzyme structure and function. *Chem. Rev.* **2014**, *114*, 3919−3962.
(71) Marcus, R. A.; Sutin, N. Electron transfers in chemistry and biology. *Biochim. Biophys. Acta, Rev. Bioenerg.* **1985**, *811*, 265−322.
(72) Dimarogona, M.; Topakas, E.; Olsson, L.; Christakopoulos, P. Lignin boosts the cellulase performance of a GH-61 enzyme from Sporotrichum thermophile. *Bioresour. Technol.* **2012**, *110*, 480−487.
(73) Westereng, B.; Cannella, D.; Wittrup Agger, J.; Jørgensen, H.; Larsen Andersen, M.; Eijsink, V. G. H.; Felby, C. Enzymatic cellulose oxidation is linked to lignin by long-range electron transfer. *Sci. Rep.* **2016**, *5*, 18561.
(74) Brenelli, L.; Squina, F. M.; Felby, C.; Cannella, D. Laccase-derived lignin compounds boost cellulose oxidative enzymes AA9. *Biotechnol. Biofuels* **2018**, *11*, 10.
(75) Couturier, M.; Ladeveze, S.; Sulzenbacher, G.; Ciano, L.; Fanuel, M.; Moreau, C.; Villares, A.; Cathala, B.; Chaspoul, F.; Frandsen, K. E.; Labourel, A.; Herpoel-Gimbert, I.; Grisel, S.; Haon, M.; Lenfant, N.; Rogniaux, H.; Ropartz, D.; Davies, G. J.; Rosso, M. N.; Walton, P. H.; Henrissat, B.; Berrin, J. G. Lytic xylan oxidases from wood-decay fungi unlock biomass degradation. *Nat. Chem. Biol.* **2018**, *14*, 306−310.
(76) Wang, B.; Li, C.; Dubey, K. D.; Shaik, S. Quantum mechanical/molecular mechanical calculated reactivity networks reveal how cytochrome P450cam and Its T252A mutant select their oxidation pathways. *J. Am. Chem. Soc.* **2015**, *137*, 7379−7390.
(77) Solomon, E. I.; Heppner, D. E.; Johnston, E. M.; Ginsbach, J. W.; Cirera, J.; Qayyum, M.; Kieber-Emmons, M. T.; Kjaergaard, C. H.; Hadt, R. G.; Tian, L. Copper active sites in biology. *Chem. Rev.* **2014**, *114*, 3659−3853.
(78) Simmons, T. J.; Frandsen, K. E. H.; Ciano, L.; Tryfona, T.; Lenfant, N.; Poulsen, J. C.; Wilson, L. F. L.; Tandrup, T.; Tovborg, M.; Schnorr, K.; Johansen, K. S.; Henrissat, B.; Walton, P. H.; Lo Leggio, L.; Dupree, P. Structural and electronic determinants of lytic polysaccharide monooxygenase reactivity on polysaccharide substrates. *Nat. Commun.* **2017**, *8*, 1064.


DOI: 10.1021/acscatal.9b00778
*ACS Catal.* 2019, 9, 4958−4969